

# Analysis and classification of power quality disturbances using variational mode decomposition and hybrid particle swarm optimization

Husham Idan Hussein<sup>1,2</sup>, Ahmed Majeed Ghadban<sup>1,2</sup>, Alejandro Rodríguez Gómez<sup>1</sup>,  
Francisco Jesus Muñoz Gutierrez<sup>1</sup>

<sup>1</sup>Electrical Engineering Department, University of Malaga, Malaga, Spain

<sup>2</sup>Electrical Power and Machines Department, College of Engineering, University of Diyala, Diyala, Iraq

## Article Info

### Article history:

Received Feb 14, 2024

Revised May 6, 2024

Accepted May 12, 2024

### Keywords:

Harmonics analysis

Power disturbances

Power quality

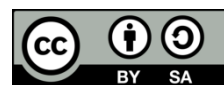
Signals processing

Transformation

## ABSTRACT

Power quality disturbances (PQD) threaten electrical power systems, especially in distributed generation with renewable energy sources and in smart grids where PQD takes a complex form. Providing accurate information on the status and characteristics of the electrical signal facilitates the identification of practical solutions to this threat. In this paper, a variational mode decomposition (VMD) signal processing tool is proposed to analyze complex PQD. In VMD, the input signal is decomposed into different band-limited intrinsic mode functions (IMF) or non-recursively reconstructed modes. The input signal analysis by VMD, which considers the frequency values and spectral decomposition for each mode, describes the changes in the input waveform, and the IMFs help extract the behavioral patterns of these disturbances. A new hybrid particle swarm optimization-technique for order of preference by similarity to ideal solution (PSO-TOPSIS) algorithm is also proposed to classify the disturbances based on the features extracted from the signals decomposed using VMD. The performance of this method is then extensively validated by using different PQDs (including complex, stationary, and non-stationary (PQDs) and through a comparison with deep learning methods, such as convolutional and recurrent neural networks. Results show that VMD has several advantages over Fourier, wavelet, and Stockwell transforms, such as its lack of any modal aliasing effect, its capability to diagnose disturbances across four noise levels, and its ability to separate harmonics from other events. The proposed VMD in combination with PSO-TOPSIS performs more accurately than the other methods across all noise levels.

This is an open access article under the [CC BY-SA](https://creativecommons.org/licenses/by-sa/4.0/) license.



## Corresponding Author:

Alejandro Rodríguez Gómez

Electrical Engineering Department, University of Malaga

Dr. Ortiz Ramos s/n, 29071- Malaga, Spain

Email: arodriguezg@uma.es

## 1. INTRODUCTION

The recent high penetration of renewable energies, such as solar and wind power, has increased the significance of power quality (PQ). However, due to their inherent variability, integrating these intermittent energy sources into electrical grids poses new challenges. In addition, the proliferation of power-electronics-based devices and non-linear loads, including electronic equipment and motor drives, introduces harmonics, voltage fluctuations and transient issues that can have undesirable effects, such as equipment malfunctions, energy losses, and increased operational costs. To address these concerns, PQ analysis techniques have been

developed to ensure the reliable and efficient operation of electrical systems while minimizing adverse effects on the grid and connected devices [1]. Amongst various PQ disturbances (PQD), harmonics have been analyzed using time-frequency transforms, such as Fourier transform (FT) [2], whose inherent limitations are addressed by wavelet transform (WT), which is an extremely useful tool for detecting and extracting valuable information for formulating digital solutions to these disturbances [3]. WT also provides an adaptive window for analyzing signal frequencies (wide and narrow windows at low and high frequencies, respectively), thus making this tool suitable for evaluating non-stationary disturbances [4]. However, WT becomes unstable under very high noise [5]. As a generalized form of FT, Stockwell transform (ST) encompasses the continuous WT and overcomes some of its disadvantages [6]. Accordingly, ST has been applied as a feature extraction tool for solving PQD [7] and has been combined with different artificial intelligence (AI) techniques, such as artificial neural networks [8], fuzzy logic [9], decision tree [10], and expert system [11], to classify such disturbances. Some scholars have localized PQD using dyadic orthonormal WT and compared the application of WT with that of ST in analyzing the PQD for integrated power systems [12]. Another technique that has gained significant attention is empirical mode decomposition (EMD) and its association with Hilbert transform (HT) [13]. EMD is a powerful approach for analyzing time series that recursively separates a signal into different band-limited, intrinsic mode functions (IMF) and estimates lower and upper wrappers via interpolation to capture their local characteristics. These IMFs are generated by using HT to directly extract the energy associated with various time scales, the local power and the instantaneous frequency. Whilst EMD has been proven effective in handling non-linear and non-stationary signals, this technique faces some limitations, such as its sensitivity to noise and sampling. Nevertheless, significant advancements in enhancing the performance and applicability of EMD have been reported in recent years. For instance, optimization constraints were incorporated into EMD to enhance its decomposition accuracy [14]. A multicomponent proximal algorithm was also proposed to further improve the decomposition quality of EMD [15]. An adaptive data analysis technique using sparse time-frequency representation was proposed in [16] to produce an efficient representation of time-varying patterns. An entirely non-recursive variational mode decomposition (VMD) model was proposed in study [17] to identify an ensemble of modes and their respective center frequencies. These modes are extracted concurrently, and the signal is reproduced collectively, with each mode becoming smooth after demodulation into the baseband. VMD can effectively mitigate mode mixing, enhance the interpretability of the extracted modes and be combined with various AI techniques. In PQ event classification, a combined VMD-SVM-based feature selection method was proposed in [18] to effectively extract discriminative features from PQ signals that are used as inputs to an SVM and to enhance the accuracy of event classification. A VMD-based feature extraction and heuristic feature selection approach for PQD recognition was also proposed in [19], whilst VMD and detrended fluctuation analysis were applied in [20] to classify PQDs in distribution networks. The technique for order of preference by similarity to ideal solution (TOPSIS) is a multi-criteria decision analysis method based on the concept of geometric distance where the chosen alternative should have the shortest distance from the positive ideal solution and the longest distance from the negative ideal solution [21]. An improved TOPSIS based on rank sum ratio was used in [22] to solve the complexity and randomness of the PQ assessment problem. An innovative closed-loop analysis framework was introduced in [23] to streamline the PQD analysis process and enhance its accuracy. Known for its remarkable performance in various tasks, including image classification, speech recognition and machine translation, deep learning automatically extracts spatial and temporal features through multiple levels of abstraction. Deep neural networks, which are equipped with specialized layers and trained on diverse samples, can autonomously extract features without going through conventional signal processing steps [24]. Deep neural networks also outperform artificial feature engineering in speech recognition and image classification. Using deep learning in solving PQDs not only enhances classification accuracy but also reduces human effort and simplifies the overall process [25].

The contribution of this work lies in its application of a new PSO-TOPSIS hybrid method for classifying PQDs based on a set of features that are extracted from the output vectors of VMD. This hybrid model is developed in two steps. Firstly, the PSO algorithm finds the weights. Secondly, these weights are integrated into TOPSIS to determine the class of each disturbance. In the proposed PSO-TOPSIS framework, numerous features are extracted from extensive disturbance samples to significantly enhance visibility. Results of comparative analyses with leading-edge intelligent techniques, including convolutional neural networks (CNN) and recurrent neural networks (RNN), and with conventional methodologies demonstrate that the proposed model effectively addresses the shortcomings inherent in traditional signal processing and artificial feature selection.

The rest of this paper is organized as follows. Section 2 introduces the materials and methods and introduces the proposed algorithms for analyzing and classifying complex PQD (CPQD) issues. Section 3 analyses PQD through case studies, examples and validation. Section 4 presents the classification results. Section 5 concludes the paper.

## 2. METHOD AND MATERIALS

### 2.1. Non-recursive variational mode decomposition (VMD)

Variational mode decomposition (VMD) works non-recursively to analyze any signal, and this model depends on the central frequency of that signal or the sub-band [26]. HT adapts all modes ( $u_k$ ) in the spectral domain (SD), and each mode function is adjusted on a single side using sub-bandwidth (1). After applying HT, the frequency spectrum modes shift to the base of the band. The center frequency ( $w_k$ ) is then adjusted based on exponential duration, and the width of the main band is determined based on the Gaussian softness of the demodulated complex signal (using the squared L2-norm of the gradient) [27], [28]. This VMD process solves variational issues (2) by employing the alternate direction method of multipliers to find the saddle point Lagrangian and to obtain all mode functions that tune the center frequency in the SD (3) and (4).

$$u_k^+(t) = \left( \delta(t) + j/\pi t \right) * u_k(t) \quad (1)$$

$$\min \left\{ \sum_{k=1}^k \|\partial[(\delta(t) + j/\pi t) * u_k(t)] e^{-jw_k t}\|_2^2, \sum_{k=1}^k u_k(t) = f(t) \right\} \quad (2)$$

$$\mathcal{L}(\{u_k\}, \{W_k\}, \lambda) = \alpha \sum_{k=1}^k \|\partial[(\delta(t) + j/\pi t) * u_k(t)] e^{-jw_k t}\|_2^2 + \|f(t) - \sum_{k=1}^k u_k(t)\|_2^2 + \langle \lambda(t), f(t) - \sum_{k=1}^k u_k(t) \rangle \quad (3)$$

$$\hat{u}_k^{n+1}(w) = \frac{\hat{f}(w) - \sum_{i < k} \hat{u}_i^{n+1}(w) - \sum_{i > k} \hat{u}_i^{n+1}(w) + \frac{\hat{\lambda}(w)}{2}}{1 + 2\alpha(w - w_k^n)^2} \quad (w > 0) \quad (4)$$

$$W_k^{n+1} = \frac{\int_0^\infty w |\hat{u}_k^{n+1}(w)|^2 dw}{\int_0^\infty |\hat{u}_k^{n+1}(w)|^2 dw} \quad (5)$$

where  $f(t)$  is the target function,  $u_k$  is denoted  $\{u_1, \dots, u_k\}$  acts all set of the decomposed modes,  $W_k$  is denoted  $\{w_1, \dots, w_k\}$  acts as the center frequencies and  $\alpha$  is the fidelity balancing factor.

### 2.2. PSO-TOPSIS method

TOPSIS is a multi-criteria decision-making method that ranks alternatives based on their relative closeness to the ideal solution. This method has been used to serve many purposes in different scientific fields. The decision matrix is a table that represents the performance of different alternatives based on multiple criteria [29], the weights represent the relative importance of each criterion in the decision-making process and the direction indicates whether each criterion should be maximized or minimized. The normalized decision matrix is multiplied by the weight vector to assign a relative weight to each criterion, and the distance to the ideal and worst-case solutions is calculated by taking the Euclidean distance between each alternative and the ideal solution. These alternatives are then classified according to their relative closeness to the ideal solution, and the best alternative has the shortest distance to the ideal solution.

The PSO algorithm is integrated with TOPSIS to find the required weights for ensuring a fast and accurate PQD classification. The PSO-TOPSIS algorithm combines the PSO optimization algorithm with the TOPSIS multi-criteria decision-making method to solve optimization problems with multiple criteria as shown in Figure 1. PSO and TOPSIS are integrated in the following steps:

Step 1: Initialize the steps of each particle (population size, max iterations, initial position, and velocity).

Step 2: Evaluate the fitness of each particle by calculating its TOPSIS score based on objective and criteria weights:

- Define the path of each criterion: The direction indicates whether each criterion should be maximized or minimized. For instance, a higher value for voltage magnitude and a lower value for voltage THD are generally preferred.
- Normalize the decision matrix: Each column of the decision matrix is normalized to have a unit vector length and to ensure that each criterion is equally vital in the decision-making process.
- Calculate the weighted normalized decision matrix: The normalized decision matrix is multiplied by the weight vector to assign a relative weight to each criterion.

Step 3: Update the step (velocity and position) of each particle based on (6) and (7).

Step 4: Re-evaluate the fitness of each particle based on the updated positions.

Step 5: Update the best position of each particle and the global best position:

- Calculate the ideal and worst-case solutions: The ideal and worst-case solutions represent the best and worst possible performances for each criterion, respectively. These two solutions are calculated by taking

the maximum and minimum values for each column of the weighted normalized decision matrix, respectively.

- Calculate the distance to the ideal and worst-case solutions: The distance to the ideal and worst-case solutions is calculated by taking the Euclidean distance between each alternative and the ideal solution and that between each alternative and the worst-case solution, respectively.
  - Calculate the relative closeness to the ideal solution: The relative closeness to the ideal solution is calculated by dividing the distance to the worst-case solution by the sum of the distance to both solutions.
- Step 6: Repeat steps 3 to 5 until the maximum number of iterations reaches the optimal solution:
- Rank the alternatives: The alternatives are ranked based on their relative closeness to the ideal solution. The alternative with the highest relative closeness is considered the best alternative.

$$V_{i,j} = w * V_{i,j} + c_1 * r_1 * (p_{i,j} - x_{i,j}) + c_2 * r_2 * (p_{g,j} - x_{i,j}) \tag{6}$$

$$x_{i,j} = v_{i,j} + x_{i,j} \tag{7}$$

where  $(v_{i,j}$ , and  $x_{i,j}$ ) are the velocity and position of particle (i) in dimension (j), respectively, w is the inertia weight,  $(c_1$  and  $c_2)$  are the acceleration coefficients,  $(r_1$  and  $r_2)$  are random numbers between 0 and 1,  $(p_{i,j})$  is the best position of particle (i) in dimension (j) and  $(p_{g,j})$  is the best position amongst all particles in dimension (j).

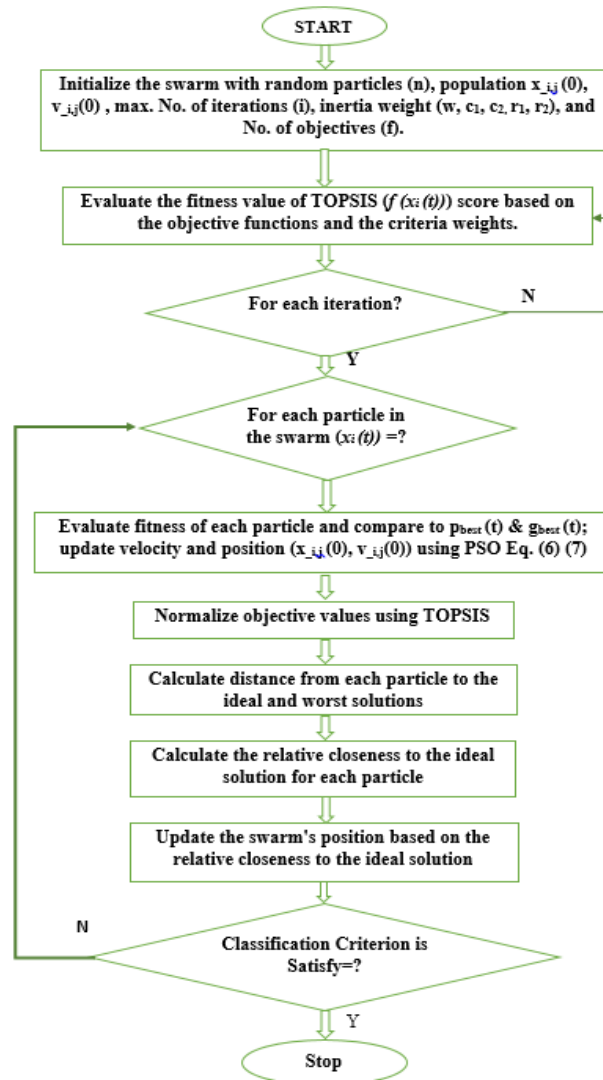


Figure 1. Flow chart of the proposed PSO-TOPSIS method

### 3. RESULTS AND DISCUSSION

Different PQDs are analyzed using VMD [30], whose performance is compared with that of other time-frequency methods, such as fast Fourier transform (FFT), WT and ST [31]. The signals are divided into two sets depending on the types of disturbances. The first set includes stationary and non-stationary cases with two disturbances and complex cases with three complex disturbances. All signals are sampled with a frequency of 6.4 kHz, the length of every signal is set to 15 cycles and a signal-to-noise ratio (SNR) varying from 40 to 20 dB is considered. VMD decomposes each signal into modes that are reconstructed non-recursively and whose number depends on the  $k$ -parameter.  $K$  is set to 3 for all cases investigated in this study. The fidelity balancing factor ( $\alpha$ ) plays an essential role as shown in (3) and is set to 1,000. Signal change is described by performing spectrum analysis for the input signal with frequency values and spectral decomposition for each mode. The frequency mode is bounded around the centre frequencies for each mode ( $k$ ) (2), and this decomposition process or minimize the effects of noise on signals and identify modes that do not contain noise (acceptable components).

#### 3.1. Stationary and non-stationary cases

##### 3.1.1. Harmonics disturbances stationary categories

Harmonics disturbances often appear in power system networks and can be viewed as examples of stationary disturbance. Harmonics distortion occurs when the signal contains different components of multiple integers of the fundamental frequency (50 Hz) and inter-harmonics. A signal with the third, fifth, seventh and ninth harmonics components is considered for the analysis in Figure 2(a). The spectral of the input signal is compared with the three decomposed modes (IMFs) in Figure 2(b) to Figure 2(c). Given that these IMFs have different central frequencies and no weaknesses (e.g. signal distortion), the input disturbance can be successfully decomposed. Figure 2(e) to Figure 2(g) illustrate the decomposition modes, which provide information about the fluctuations that may appear suddenly as disturbances on the signal, Figure 3(a) to Figure 3(b) shows the time-frequency analysis results for the harmonics disturbance as obtained using ST and FFT and Figure 4 presents the WT analysis of the signal and the details of coefficients at five levels (d1 to d5). The decomposition modes signals by WT correspond to the behavior of the harmonic that may be combined with the PQDs.

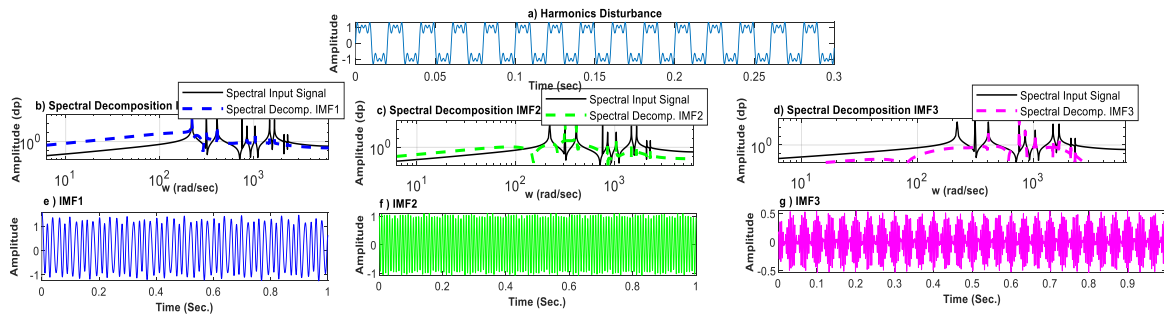


Figure 2. Harmonics disturbance signal: (a) Harmonics disturbance signal in time series, (b) spectral input signal (solid line) compared with frequency IMF1 (blue dashed line), (c) spectral input signal (solid line) compared with frequency IMF2 (green dashed line), (d) spectral input signal (solid line) compared with frequency IMF3 (pink dashed line), and (e)–(g) decomposed information for IMF1–IMF3

##### 3.1.2. Oscillatory transient disturbance non-stationary category

The oscillatory transient disturbance taking place in various sections of a power system network shows distinct features, including a brief duration and significant voltage amplitude and frequency fluctuations. Figure 5(a) presents the results of VMD analysis of an oscillatory transient disturbance lasting for 0.055 to 0.064 s. Figures 5(b) to 5(d) present the decomposition of frequencies and their centering around the central frequency, whilst Figures 5(e) to 5(g) present other data that may be relevant to the VMD IMFs decomposition, including the starting and ending disturbance times and the values of magnitude and other accompanying components.

Stockwell transform (ST) is more suitable than FFT for analyzing oscillatory transients given that the former provides a time-frequency representation that precisely captures transient behavior, including the time localization and frequency of oscillatory transient disturbance. By contrast, FFT is more suitable for steady-state signals but does not offer the same level of detail for transient analysis. Figure 6 presents the

results of ST disturbance analysis starting at 0.05 s, where the yellow color denotes the extreme area starting from 0.01 when the frequency rises to 150 Hz, the signal is cut and forms in ST performance. The corresponding ST and FFT are shown in Figures 6(a) and 6(b). WT identifies and establishes the swell with harmonic conditions by using the mother wavelet of the Haar function (d1, d5) as shown in Figure 7. Whilst the results obtained using the above methods perfectly match one another, VMD outperforms all other methods given its ability to extract a huge amount of information that helps in quickly finding solutions to PQ problems.

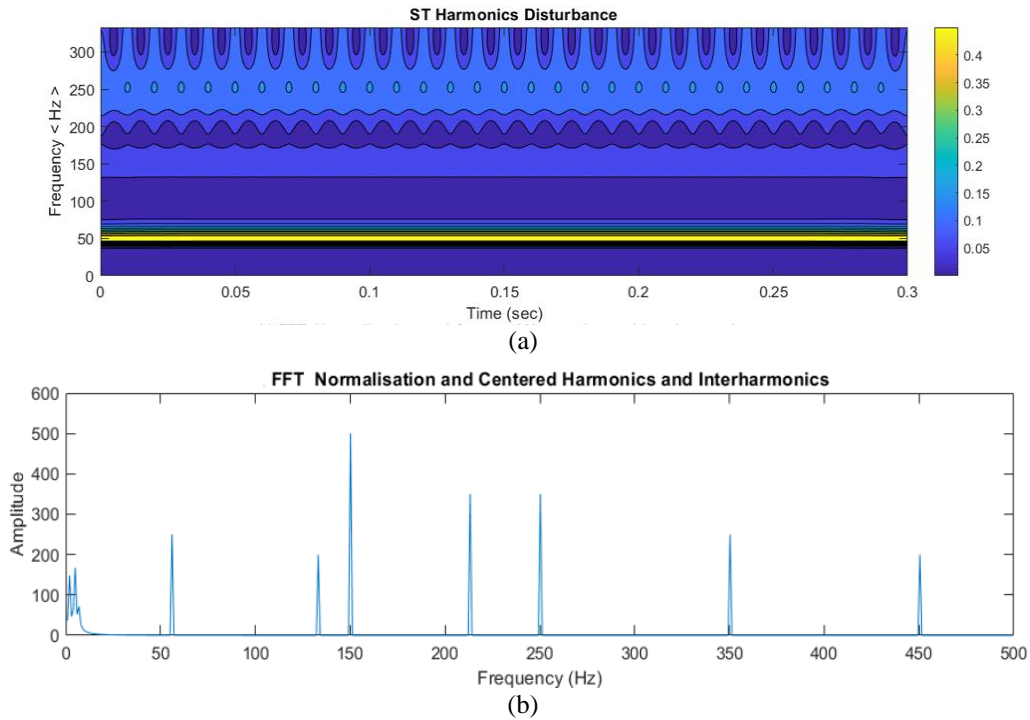


Figure 3. Harmonics disturbance signal: Signal analysis within 15 cycles using ST and FFT (a) Harmonics disturbance in the ST simulation starting at 0–0.3 s. The yellow color indicates the value of 50 Hz and confirms the frequency in graph (b). (b) The FFT normalization and center ( $\omega_k$ ) of the absolute value

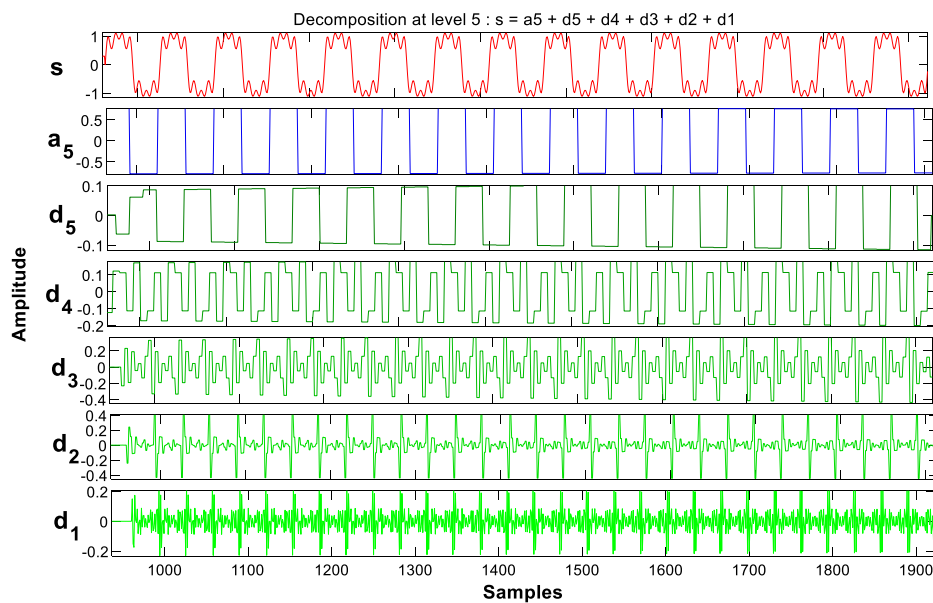


Figure 4. WT decomposition of the harmonics disturbance signal

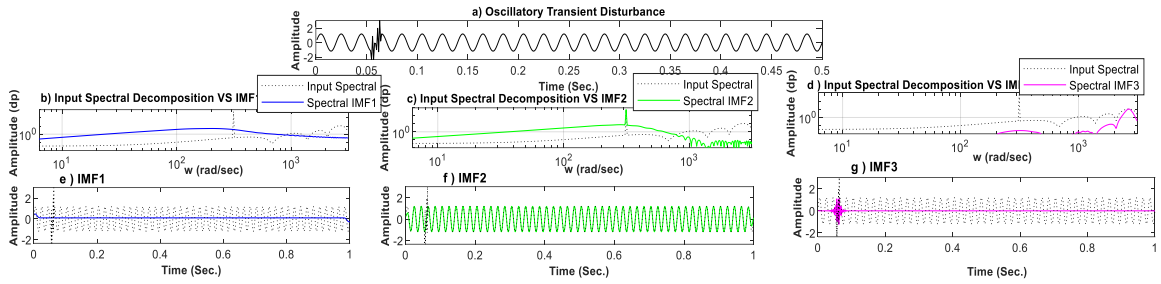


Figure 5. VMD decomposition of oscillatory transient disturbance: Three modes extracted by VMD within  $K=3$ . (a) Oscillatory transient disturbance signal in time series after 15 cycles, (b)–(d) spectral input disturbance signal against the spectral of the decomposed IMFs. (e)–(g) the decomposed modes IMF1 (starting and ending times), IMF2 (magnitude) and IMF3 (transient) for oscillatory transient disturbance

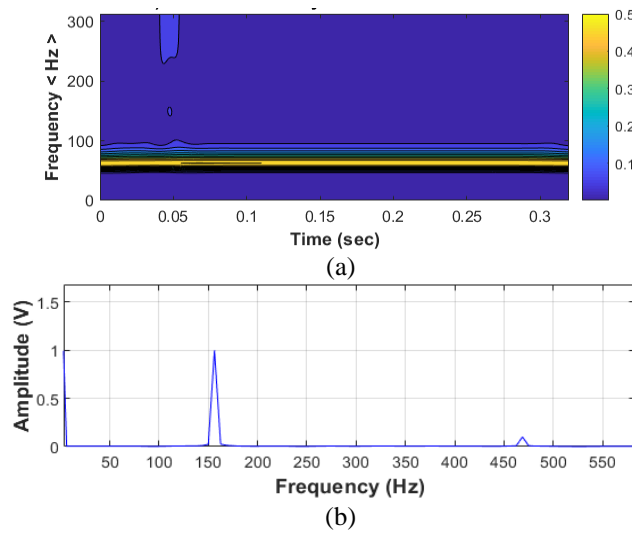


Figure 6. Oscillatory transient disturbance signal after 15 cycles (a) Analysis signal of oscillatory transient disturbance as captured by ST, and (b) FFT normalization and center of the absolute value

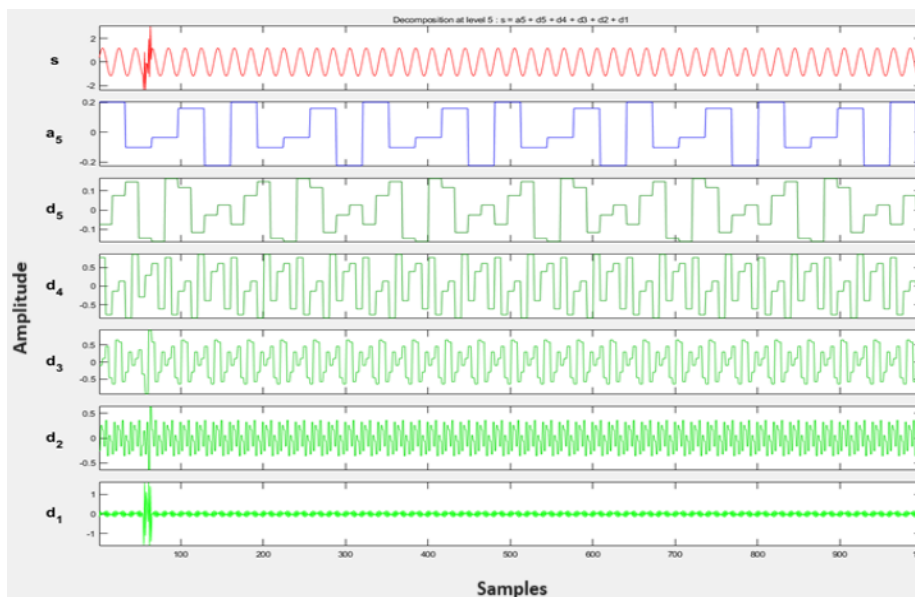


Figure 7. WT decomposition of the oscillatory transient disturbance signal

**3.2. Complex disturbances cases**

**3.2.1. Sag with harmonics disturbances**

Figure 8(a) shows a CPQD sag with harmonics as a non-stationary category with  $(\alpha)=1,000$ . The voltage sag with a harmonic of 40% is used as a disturbance signal. Depending on this disturbance signal, the amplitude of the maximum frequency appears shortly with a frequency of 50 Hz. Therefore, this frequency can be used to concentrate the beginning and end of the voltage sag 40% and the harmonic (0 to 0.3 s) and to detect the disturbance by diagnostic signal decreased from 0.05 to 0.15 and then increasing to the peak values of high frequency at 0.0158 sec. The VMD model has extracted modes or IMFs based on  $K=3$ . Figure 8(b) shows the spectrum of the input signal, which has noises and transitions, Figure 8(c) presents a spectral comparison between the input signal and the decomposed modes and Figures 8(d) to 8(e) show the local characteristics of the highly non-stationary CPQD signals. Each IMF is accompanied by a similar number of extrema and zero-crossing and is symmetrical around the local mean. The first mode shows the signal in time series, whilst the second mode presents the start and end of the disturbance signal. The harmonics in the last mode have been decomposed as shown in Figure 8(f).

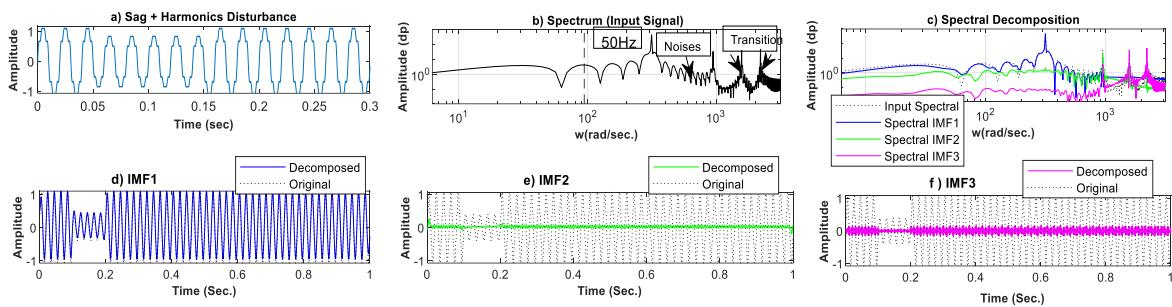


Figure 8. VMD decomposition sags with harmonics disturbance (a) Sag with harmonics disturbance single analysis, (b) spectrum input signal with 50 Hz, (c) spectral decomposition comparison, and (d)–(f) IMF1, IMF2 and IMF3, respectively

**3.2.2. Swell with harmonics disturbances**

Swell with harmonics disturbances is a complex PQ issue. The VMD dataset should be appropriately arranged with  $(k)$  number of modes and balancing factor  $(\alpha)$ , which are essential factors that may affect the convergence or clarity of the PQD signal modes. The magnitude of the swell reaches 1.6 pu between 50 and 150 ms at 50 Hz (fundamental frequency) and a sampling frequency 6,400 Hz with a brief increase in power. The RMS increases from 1 to 1.2 pu starting at 50 ms for a duration of 100 ms. Figure 9(a) to Figure 9(c) show the spectral decomposition for each IMF compared with the spectral of the input signal for the swell with harmonics disturbance simulated by VMD. The corresponding frequencies are clear and distributed around the center frequency  $(\omega_k)$ . The decomposition includes three modes Figure 9(d) to Figure 9(f) covering the form of the swell disturbance, the boundaries of the signal and the harmonics components.

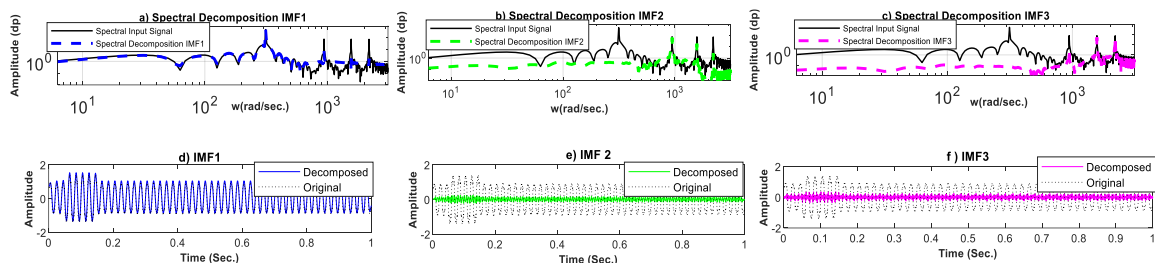


Figure 9. VMD decomposition of swells with harmonics disturbance: (a)–(c) decomposed spectra for each IMF before preprocessing and after preprocessing. Each frequency for IMFs is distributed around the center frequency  $(\omega_k)$ . (d)–(f) present the reconstructed modes, such as the magnitude of swell, the boundary of disturbance and the harmonics distortion



### 3.2.3. Interruption with harmonics disturbances

Figures 10(a) to 10(f) show the VMD analysis results for interruption with harmonics disturbance. IMF1 to IMF3 are decomposed and compared with the original input signal. The signal is then decomposed into three intrinsic mode functions and a residual component. Each IMF represents a specific frequency component of the signal, and the residual component captures any remaining components that these IMFs cannot represent. In the case of interruption with harmonics disturbance, the starting time of the process increases from 0.05 to 0.15 s. VMD analyses the signal associated with the starting time and decomposes this signal into frequency components to provide insights into the presence of different frequency components, including harmonics, in this signal. The specific characteristics of each IMF can be analyzed to identify the impact of harmonics on the starting time. The changes in the IMFs obtained from the VMD decomposition can be compared before and after the harmonics disturbance to observe any shifts or alterations that may explain the delay in the starting time. The residual component can also provide information about any remaining components that may contribute to the interruption. The effectiveness of VMD and the selection of  $K=3$  depend on the specific characteristics of the signal and the nature of the harmonics disturbance.

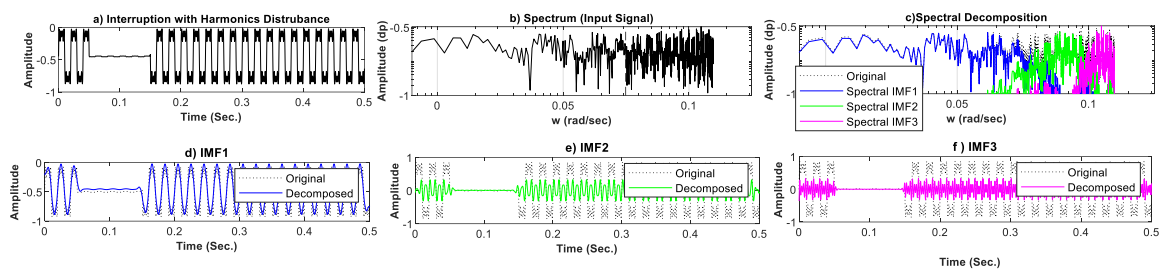


Figure 10. VMD decomposition of interruption with harmonics disturbance and  $K=3$ . (a) Interruption with harmonics disturbance signal, (b) input signal spectrum, (c) comparison between input spectral signals and the decomposed signals, and (d)–(f) IMF1, IMF2 and IMF3 for interruption with harmonics disturbance, respectively

### 3.3. Validation cases

Six types of PQDs including the normal sine wave are arranged as normal sag, interruption, swell, impulsive transient disturbance and flicker. Figures 11(a) to 11(c) present the normal signal with 50 Hz in time series, and by applying VMD, the modes are extracted with  $K=3$ , the spectral of the input signal and the frequency of the IMFs decomposed and distributed around the center frequency ( $\omega_k$ ). No harmonic components are detected in the analysis. Figure 12 presents the results of the resolution analysis for the sag disturbance that is modelled mathematically and simulated by VMD. These results show the high accuracy and efficient mode extraction of VMD. Figure 12(a) presents the signal in time series while the Figures 12(b) to 12(c) present a spectral comparison of the input and the decomposed IMFs. As one advantage of VMD, the analyzed frequencies are centered around the central frequency, thus ultimately containing the wave or signal without lack of variance. Figure 13(a) to 13(b) presents the results for interruption disturbance in time series and spectrum input signal and spectral decomposition for IMFs respectively. A vast amount of data is collected to identify the causes of PQD. The VMD capability shows how the modes and their frequencies are extracted, including the starting and ending interruption times and the harmonic components that may appear on the signal during the disturbance. Figures 14(a) to 14(b) show the results of the swell disturbance with VMD decomposition in time series, and the spectrum input signal with all decomposed spectral modes. Figures 15(a) to 15(c) show the results and impulsive transient disturbances analysis in time series, the spectral modes and the IMFs, respectively. The input spectral signal is compared with the decomposed IMFs, and the reconstructed modes are accurately decomposed for each IMF. Figures 16(a) to 16(c) shows the VMD decomposition of flicker disturbance with 15 cycles,  $\alpha=1,000$  and three modes. The disturbance signal in time series, spectrum input signal and the spectral decomposition modes. The high resolution of the decomposition is very clear.

Various signal processing techniques can be employed in analyzing PQDs, including VMD, ST, FFT and WT. whilst each technique has its strengths and weaknesses, VMD emerges as the ideal method for analyzing PQ. Specifically, VMD excels in handling non-stationary signals with time-varying frequency content, thereby making this method well-suited for examining PQDs. VMD also clearly separates the signal components, thus preserving amplitude and phase information, enabling an enhanced feature extraction and

interpretation and facilitating the identification and characterization of different types of disturbances. Although computationally more intensive, the ability of VMD to capture subtle variations and transient events in power signals makes this method valuable in PQ analysis.

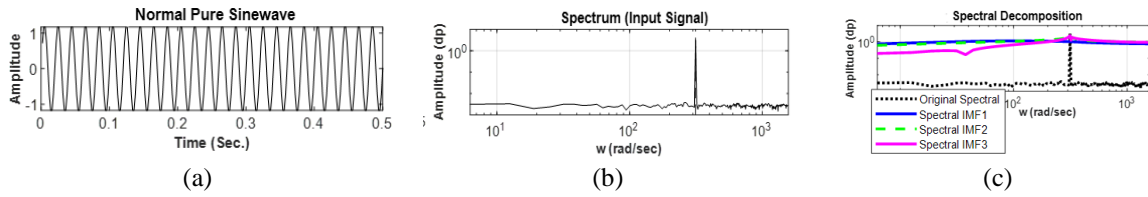


Figure 11. VMD decomposition of normal pure sine wave signal (a) Normal pure sine wave single in time series, (b) spectrum input signal at 50 Hz, and (c) spectral decomposition for each decomposed mode

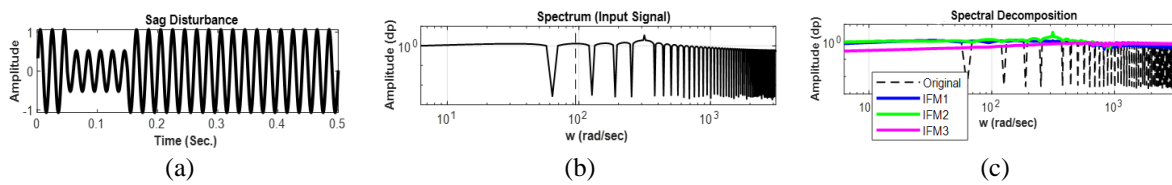


Figure 12. VMD decomposition of sag disturbance (a) Sag disturbance signal in time series, (b) comparison of the spectrum input signal with the spectral modes decomposition, and (c) comparison of the IMF1-IMF3 spectral and the original spectral

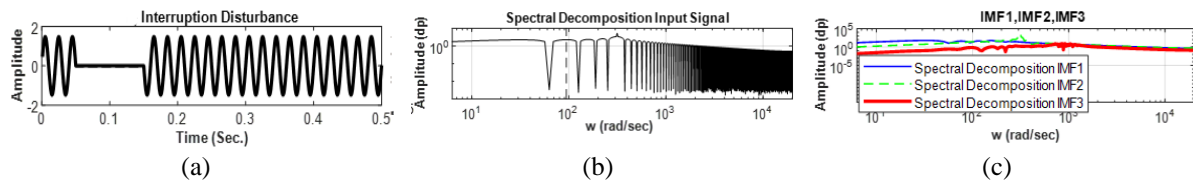


Figure 13. VMD decomposition of interruption disturbance (a) Interruption disturbance signal in time series, (b) spectrum input signal and spectral decomposition for IMFs, and (c) IMF1, IMF2, IMF3

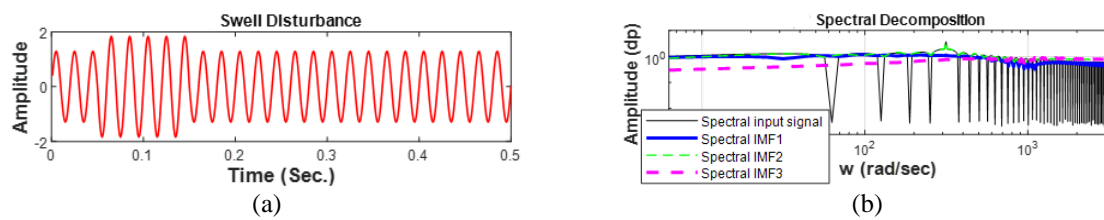


Figure 14. VMD decomposition of swell disturbance (a) swell disturbance signal in time series and (b) spectrum input signal with all decomposed spectral modes

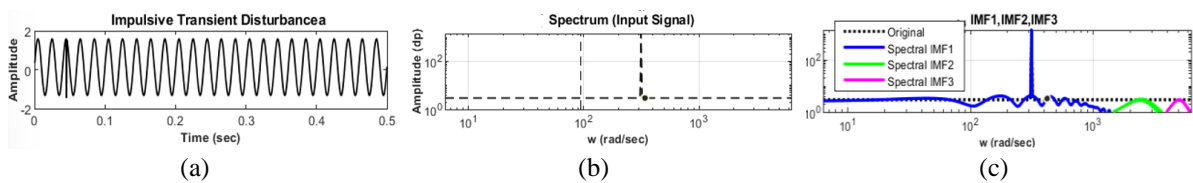


Figure 15. VMD decomposition of impulsive transient disturbance. Three modes should be extracted by VMD within  $K=3$ : (a) Impulsive transient disturbance signal in time series, (b) spectrum input signal at 50 Hz, and (c) spectral decomposition for decomposed IMF1, IMF2, and IMF3 for impulsive transient disturbance

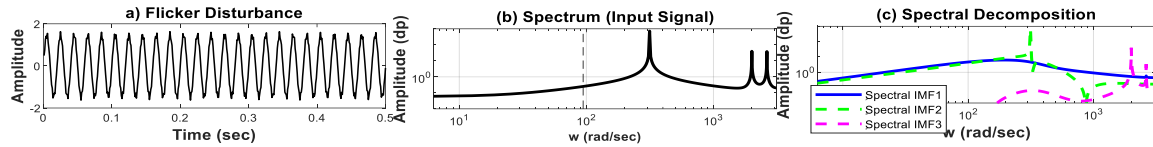


Figure 16. VMD decomposition of flicker disturbance with 15 cycles,  $\alpha = 1000$  and three modes: (a) Flicker disturbance signal in time series, (b) spectrum input signal, and (c) spectral decomposition for modes

#### 4. CLASSIFICATION RESULTS

The IEEE standard 1159-1995 is used in this study due to the difficulty in accessing data for PQD classification [32], [33]. Similar to other studies, a preliminary simulation is conducted to obtain the best classification of PQDs. As shown in Figure 17, PSO-TOPSIS classifies PQDs into normal pure, impulsive transient, oscillatory transient, swell with harmonics, harmonics, interruption with harmonics, sag with harmonics, flicker, sag, interruption and swell, which are denoted by C0 to C10, respectively. All signals have a 50 Hz fundamental frequency, the number of samples per cycle is 128 and each signal has a duration of 15 cycles. Therefore, every signal consists of 1920 samples. As inputs for PSO-TOPSIS, each class contains 100 cases out of 100 signals used for PQD classification after feature selection. All signals generated from these classes are presented in each part of the results and evaluated for all methods to measure and compare their accuracy. The MATLAB package [34], [35] has been used to achieve the results. The PQD classification is performed in four steps. Firstly, the mathematical equations model is used to form all PQDs. Secondly, a computerized vision is applied to generate signals or waveforms of the disturbances to analyze these disturbances and to extract essential data for explaining the disturbances matrix. VMD decomposes each signal into several IMFs or modes whose number can be controlled through K, which is set to 3 in this paper. These IMFs are then used as vector inputs for normalization and classification. The ST matrix contains complex elements, including rows and columns that denote frequencies and time, respectively. The maximized elements in each row and column produce magnitude and frequency contours that are used as input vectors for PSO-TOPSIS. WT is ideal for analyzing non-stationary PQD signals, whilst FFT is ideal for analyzing stationary signals, such as sinusoidal ones. The input vectors of each method are fed into PSO-TOPSIS one by one. Thirdly, the feature selection is normalized. This step considers the disturbance duration and frequency range, the computational complexity, the sampling rate and the noise level. Eleven features are selected to cover all signal characteristics, namely, total harmonic distortion (THD), root mean square (RMS), mean, standard deviation, max value, min value, energy of frequency, kurtosis index, skewness, variance and range, which are applied to each signal in each method. The final input matrix becomes a  $[11 \times 11]$  matrix that can be combined with PSO-TOPSIS to classify the disturbances based on these features. The last step is divided into two parts. Firstly, the necessary weights are obtained using the PSO algorithm, and these weights are fed into TOPSIS to classify PQDs. To illustrate the accuracy of the proposed method after modes decomposition under noisy environments, SNR is added to each signal and then tested at 40, 35, 30 and 20 dB. VMD obtains an accuracy of 98%–90%, which is higher than those obtained by ST (97.5%–87.5%), FFT (96%–87%) and WT (95%–85.6%). As shown in Table 1, the accuracy rates for 20 dB SNR are much lower than those for the other levels due to the large number of fluctuations in this level. The SNR in PSO-TOPSIS is 90%, which is higher than that obtained by the other methods. VMD then obtains the highest accuracy in decomposing PQDs under the presence of large fluctuations, thus giving this model an edge in classification under different SNR situations. The SNR is defined using (8).

$$SNR = 10 \log \frac{P_s}{P_n} \quad (8)$$

where  $P_s$  is the original signal power, and  $P_n$  is the noise power.

As shown in Table 2, the CNNs for (VMD and ST) and (FFT and WT) demonstrate strong capabilities under various SNR levels, with (VMD and ST) achieving a slightly higher average accuracy of 96% compared with (FFT and WT), which only has an accuracy of 90.7%. Whilst (FFT and WT) excels at 40 dB SNR with 100% accuracy, (VMD and ST) closely follows with 99% accuracy. The best accuracy for (VMD and ST) is marginally higher than that for (FFT and WT) (99% vs. 98%). The choice between these two methods should depend on specific application requirements, with (VMD and ST) generally offering higher average accuracy and (FFT and WT) demonstrating exceptional performance at higher SNR levels. Table 3 shows that the RNNs for (VMD and ST) and (FFT and WT) exhibit robust capabilities under varying SNR levels. The average accuracy for (VMD and ST) stands at 94.5%, with the highest accuracy (97.8%) obtained in the normal class, whilst the average accuracy for (FFT and WT) stands at 88.5%, with the highest

accuracy (99%) also obtained in the normal class. (VMD and ST) maintains higher accuracy across all SNR levels, demonstrating its consistent and reliable performance, whilst (FFT and WT) displays competitive accuracy with some peaks in several scenarios. The choice between these methods should depend on the specific application requirements, with (VMD and ST) offering higher overall accuracy and (FFT and WT) showcasing a notable performance under certain conditions.

PSO-TOPSIS with VMD achieves an accuracy ranging from 98%–90%, which is much higher than those obtained by ST (97.5%–87.5%), FFT (96%–87.5%) and WT (95%–85.6%). The CNNs and RNNs for (VMD and ST) and (FFT and WT) exhibit strong capabilities under diverse SNR conditions. Specifically, (VMD and ST) achieves a slightly higher average accuracy than (FFT and WT) (96% vs. 90.7%). Whilst (FFT and WT) excels at 40 dB SNR with 100% accuracy, (VMD and ST) closely follows with 99% accuracy. The RNNs for (VMD and ST) maintain a higher average accuracy of 94.5%, with notable peaks at 97.8%, whilst those for (FFT and WT) achieve an average accuracy of 88.5%, with exceptional accuracy at 99%. The choice between these methods depends on specific application requirements, with (VMD and ST) generally providing higher accuracy across different SNR levels and (FFT and WT) showing a notable performance in specific scenarios.

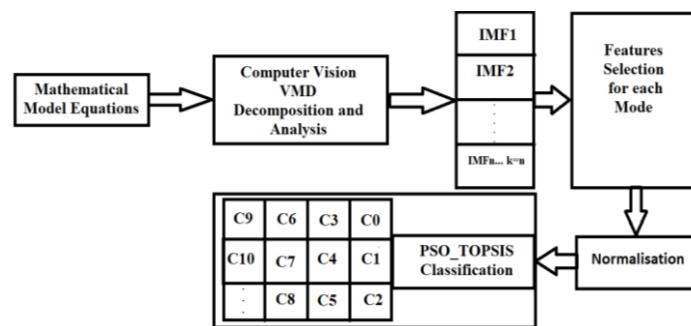


Figure 17. General block diagram of PSO-TOPSIS

Table 1. Comparison of accuracy percentage for (VMD and ST) and (FFT and WT) with different levels of SNR (in dB) using PSO-TOPOSIS

| PQDs      | CL        | VMD   |       |       |       | ST    |       |       |       | FFT   |       |       |       | WT    |       |       |       |       |
|-----------|-----------|-------|-------|-------|-------|-------|-------|-------|-------|-------|-------|-------|-------|-------|-------|-------|-------|-------|
|           |           | 40 db | 35 db | 30 db | 20 db | 40 db | 35 db | 30 db | 20 db | 40 db | 35 db | 30 db | 20 db | 40 db | 35 db | 30 db | 20 db |       |
| Normal    | C0        | 100   | 99    | 97    | 90    | 99    | 97    | 95    | 84    | 98    | 97    | 96    | 89    | 99    | 97    | 95    | 84    |       |
|           | IT        | C1    | 97    | 97    | 99    | 89    | 98    | 94    | 97    | 90    | 98    | 94    | 87    | 98    | 94    | 97    | 76    |       |
|           | OT        | C2    | 98    | 94    | 95    | 93    | 98    | 95    | 94    | 91    | 98    | 96    | 95    | 91    | 98    | 95    | 86    |       |
|           | S+H       | C3    | 100   | 99    | 97    | 87    | 97    | 99    | 91    | 81    | 100   | 97    | 93    | 85    | 97    | 99    | 98    |       |
| Harmonics | C4        | 98    | 98    | 95    | 92    | 98    | 97    | 96    | 87    | 97    | 95    | 99    | 90    | 98    | 97    | 96    | 88    |       |
|           | Int+H     | C5    | 99    | 94    | 97    | 93    | 96    | 90    | 91    | 88    | 99    | 97    | 98    | 90    | 96    | 91    | 68    |       |
|           | Sag+H     | C6    | 100   | 97    | 99    | 86    | 100   | 97    | 95    | 92    | 96    | 96    | 90    | 86    | 100   | 97    | 90    |       |
|           | Flicker   | C7    | 95    | 94    | 89    | 95    | 91    | 96    | 94    | 90    | 91    | 84    | 96    | 90    | 91    | 96    | 91    |       |
|           | Sag       | C8    | 95    | 99    | 90    | 92    | 93    | 90    | 92    | 82    | 94    | 92    | 93    | 93    | 93    | 90    | 85    |       |
| Interrupt | C9        | 100   | 94    | 92    | 90    | 93    | 95    | 92    | 91    | 98    | 99    | 90    | 78    | 93    | 95    | 92    | 93    |       |
|           | Swell     | C10   | 98    | 96    | 95    | 85    | 94    | 91    | 95    | 86    | 95    | 93    | 94    | 83    | 94    | 91    | 83    |       |
|           | Average % |       | 98%   | 96%   | 95%   | 90%   | 97.5% | 94.7% | 93%   | 87.5% | 96%   | 94.5% | 94%   | 87%   | 95%   | 94.3% | 93%   | 85.6% |

Table 2. Performance of CNNs for (VMD and ST) and (FFT and WT) under different levels of SNR (in dB)

| PQDs      | CL        | VMD   |       |       |       | ST    |       |       |       | FFT   |       |       |       | WT    |       |       |       |       |
|-----------|-----------|-------|-------|-------|-------|-------|-------|-------|-------|-------|-------|-------|-------|-------|-------|-------|-------|-------|
|           |           | 40 db | 35 db | 30 db | 20 db | 40 db | 35 db | 30 db | 20 db | 40 db | 35 db | 30 db | 20 db | 40 db | 35 db | 30 db | 20 db |       |
| Normal    | C0        | 100   | 99    | 98    | 90    | 100   | 98    | 99    | 99    | 98    | 97    | 98    | 90    | 100   | 97    | 95    | 90    |       |
|           | IT        | C1    | 100   | 99    | 100   | 89    | 100   | 98    | 99    | 98    | 98    | 94    | 96    | 89    | 100   | 94    | 87    |       |
|           | OT        | C2    | 99    | 99    | 99    | 93    | 98    | 99    | 99    | 98    | 98    | 96    | 95    | 93    | 97    | 95    | 86    |       |
|           | S+H       | C3    | 100   | 100   | 99    | 87    | 100   | 99    | 100   | 97    | 100   | 97    | 94    | 87    | 100   | 99    | 98    |       |
| Harmonics | C4        | 100   | 100   | 100   | 92    | 100   | 96    | 100   | 98    | 97    | 95    | 99    | 92    | 100   | 97    | 96    | 90    |       |
|           | Int+H     | C5    | 97    | 98    | 97    | 93    | 99    | 97    | 98    | 96    | 99    | 97    | 98    | 93    | 100   | 90    | 87    |       |
|           | Sag+H     | C6    | 100   | 100   | 99    | 86    | 100   | 97    | 100   | 100   | 100   | 96    | 98    | 86    | 100   | 97    | 89    |       |
|           | Flicker   | C7    | 100   | 100   | 96    | 95    | 100   | 96    | 100   | 91    | 100   | 98    | 96    | 95    | 100   | 96    | 95    |       |
|           | Sag       | C8    | 98    | 99    | 100   | 92    | 97    | 95    | 99    | 93    | 99    | 98    | 97    | 92    | 99    | 90    | 80    |       |
| Interrupt | C9        | 100   | 97    | 98    | 95    | 98    | 95    | 97    | 93    | 98    | 99    | 100   | 95    | 98    | 95    | 92    | 97    |       |
|           | Swell     | C10   | 100   | 99    | 100   | 94    | 100   | 97    | 99    | 94    | 95    | 97    | 94    | 100   | 91    | 95    | 99    |       |
|           | Average % |       | 99%   | 99%   | 98%   | 91.4% | 99%   | 97%   | 99%   | 96%   | 98%   | 96.7% | 97%   | 91%   | 99%   | 94%   | 93%   | 90.7% |

Table 3. Performance of RNNs for (VMD and ST) and (FFT and WT) under different levels of SNR (in dB)

| PQDs      | CL  | VMD   |       |       | ST    |       |       | FFT   |       |       | WT    |       |       |     |     |     |       |
|-----------|-----|-------|-------|-------|-------|-------|-------|-------|-------|-------|-------|-------|-------|-----|-----|-----|-------|
|           |     | 40 db | 35 db | 30 db | 20 db | 40 db | 35 db | 30 db | 20 db | 40 db | 35 db | 30 db | 20 db |     |     |     |       |
| Normal    | C0  | 100   | 99    | 97    | 100   | 100   | 96    | 97    | 92    | 100   | 97    | 99    | 90    | 100 | 99  | 91  | 90    |
| IT        | C1  | 95    | 98    | 99    | 95    | 98    | 98    | 97    | 90    | 100   | 95    | 92    | 90    | 98  | 95  | 98  | 80    |
| OT        | C2  | 95    | 99    | 95    | 95    | 98    | 100   | 94    | 91    | 100   | 96    | 95    | 91    | 99  | 95  | 94  | 87    |
| S+H       | C3  | 100   | 99    | 97    | 100   | 100   | 99    | 89    | 90    | 100   | 96    | 95    | 90    | 100 | 98  | 92  | 100   |
| Harmonics | C4  | 98    | 98    | 95    | 98    | 98    | 97    | 96    | 97    | 96    | 94    | 99    | 93    | 98  | 97  | 94  | 90    |
| Int+H     | C5  | 100   | 95    | 97    | 100   | 96    | 90    | 90    | 90    | 99    | 97    | 99    | 90    | 100 | 92  | 91  | 77    |
| Sag+H     | C6  | 100   | 97    | 99    | 95    | 100   | 97    | 95    | 94    | 100   | 96    | 94    | 90    | 99  | 96  | 89  | 90    |
| Flicker   | C7  | 95    | 99    | 89    | 95    | 99    | 100   | 97    | 90    | 100   | 87    | 97    | 91    | 100 | 96  | 91  | 91    |
| Sag       | C8  | 95    | 99    | 90    | 100   | 99    | 90    | 92    | 98    | 100   | 92    | 90    | 90    | 98  | 90  | 90  | 86    |
| Interrupt | C9  | 100   | 100   | 92    | 98    | 98    | 100   | 93    | 97    | 97    | 99    | 90    | 89    | 100 | 95  | 99  | 92    |
| Swell     | C10 | 98    | 100   | 95    | 100   | 97    | 91    | 100   | 96    | 99    | 93    | 90    | 91    | 100 | 90  | 96  | 90    |
| Average % |     | 97.8% | 98%   | 95%   | 97%   | 98%   | 96%   | 94.5% | 93%   | 99%   | 94%   | 94.5% | 90%   | 99% | 94% | 93% | 88.5% |

## 5. CONCLUSION




This paper presents a new non-recursive VMD method that analyses PQDs, such as stationary and non-stationary signals, in several stages. All complex disturbances are mathematically modelled using MATLAB, and many features are extracted according to the VMD results to facilitate the classification of PQDs. This study also proposes the hybrid PSO-TOPSIS method for classifying PQDs based on the feature selections. Specifically, PSO chooses the required weights and then sends/feeds them to TOPSIS, which then classifies the PQDs according to the ideal distances between the features extracted from VDM. According to the classification results, priority is given to those disturbances with many fluctuations, excluding the normal ones (C0). The ability of VDM to decompose or separate complex signals into many modes or IMFs highlights its superiority over other methods for analyzing signals with different frequencies and window clarity. After separating and analyzing the components of the disturbance signal, the amplitude of the voltage signal is eliminated, and VMD confines such amplitude. VMD produces many modes with varying behaviors. Depending on the center frequency used in an environment with distortions or high noise, the responses of all magnitudes, frequencies and phases contribute to an accurate identification and analysis of PQDs. The decomposed modes that are directly related to the required signal are selected, and the interruptions, increments and decrements in the signal are identified to understand the variation time and values of those elements that affect the shape of the signal. Non-recursive VMD separates the signals for a cluster of mode functions dealing with non-recursive scheming and mode mixing disturbances. This approach can adaptively determine the frequency's band-related spectral decomposition and spectrum and estimates the corresponding modes simultaneously. These features demonstrate the ability of the time-frequency approach using ST, FFT, and WT, all of which are considered powerful tools for analyzing CPQDs. ST reduces the number of samples used in signals, thus reducing the mathematical operations and computational steps whilst increasing efficiency. Unlike in WT, the phase information provided by ST is connected to the origin in time. Results show that ST can identify noise disturbances or transient states in the waves, whereas WT cannot obtain similar results due to its sensitivity to noise. However, ST has two drawbacks. The first drawback is related to the DC component of the exponential decay ( $Hz=0$ ) because this approach cannot analyze the DC change in time and only considers the average length of the analyzed signal. The second drawback is related to high frequencies, where the window is very narrow, thus reducing the number of signal samples to be analyzed by ST. This drawback may reduce the frequency accuracy and time quality. The accuracy of ST has been tested under a noisy environment. Compared with deep learning methods, the CNNs for (VMD and ST) and (FFT and WT) generally achieve higher average accuracy, whilst their RNNs achieve notable accuracy only in specific scenarios, particularly at 40 dB SNR.

## REFERENCES




- [1] A. A. Romero-Quete, G. O. Suvire, H. C. Zini, and G. Rattá, "Time-varying harmonic analysis of electric power systems with wind farms, by employing the possibility theory," *DYNA (Colombia)*, vol. 82, no. 192, pp. 185–194, Aug. 2015, doi: 10.15446/dyna.v82n192.48617.
- [2] A. H. Ghaemi, H. Askarian Abyaneh, and K. Mazlumi, "Harmonic indices assessment by wavelet transform," *International Journal of Electrical Power and Energy Systems*, vol. 33, no. 8, pp. 1399–1409, Oct. 2011, doi: 10.1016/j.ijepes.2011.06.020.
- [3] M. Uyar, S. Yildirim, and M. T. Gencoglu, "An effective wavelet-based feature extraction method for classification of power quality disturbance signals," *Electric Power Systems Research*, vol. 78, no. 10, pp. 1747–1755, Oct. 2008, doi: 10.1016/j.epsr.2008.03.002.
- [4] S. Santoso, E. J. Powers, W. M. Grady, and P. Hofmann, "Power quality assessment via wavelet transform analysis," *IEEE Transactions on Power Delivery*, vol. 11, no. 2, pp. 924–930, Apr. 1996, doi: 10.1109/61.489353.
- [5] J. G. M. S. Decanini, M. S. Tonelli-Neto, F. C. V. Malange, and C. R. Minussi, "Detection and classification of voltage disturbances using a Fuzzy-ARTMAP-wavelet network," *Electric Power Systems Research*, vol. 81, no. 12, pp. 2057–2065, Dec.

- 2011, doi: 10.1016/j.epr.2011.07.018.
- [6] P. K. Dash, B. K. Panigrahi, and G. Panda, "Power quality analysis using S-transform," *IEEE Transactions on Power Delivery*, vol. 18, no. 2, pp. 406–411, Apr. 2003, doi: 10.1109/TPWRD.2003.809616.
- [7] R. G. Stockwell, "Localization of the complex spectrum: the s transform," *IEEE Transactions on Signal Processing*, vol. 44, no. 4, Apr. 1996, doi: 10.1109/78.492555.
- [8] D. Granados-Lieberman, R. J. Romero-Troncoso, R. A. Osornio-Rios, A. Garcia-Perez, and E. Cabal-Yepez, "Techniques and methodologies for power quality analysis and disturbances classification in power systems: a review," *IET Generation, Transmission and Distribution*, vol. 5, no. 4, pp. 519–529, 2011, doi: 10.1049/iet-gtd.2010.0466.
- [9] A. Rodriguez, I. E. Ruiz, J. Aguado, J. J. Lopez, F. I. Martin, and F. Muñoz, "Classification of power quality disturbances using S-transform and Artificial Neural Networks," May 2011, doi: 10.1109/PowerEng.2011.6036517.
- [10] N. A. S. Zakaria, D. M. Said, N. Rosmin, N. Ahmad, M. S. S. Jamil, and S. Mirsaedi, "Comparison analysis of different classification methods of power quality disturbances," *International Journal of Electrical and Computer Engineering (IJECE)*, vol. 12, no. 6, pp. 5754–5764, Dec. 2022, doi: 10.11591/ijece.v12i6.pp5754-5764.
- [11] T. Zhong, S. Zhang, G. Cai, Y. Li, B. Yang, and Y. Chen, "Power quality disturbance recognition based on multiresolution S-transform and decision tree," *IEEE Access*, vol. 7, pp. 88380–88392, 2019, doi: 10.1109/ACCESS.2019.2924918.
- [12] L. Lin, D. Wang, S. Zhao, L. Chen, and N. Huang, "Power quality disturbance feature selection and pattern recognition based on image enhancement techniques," *IEEE Access*, vol. 7, pp. 67889–67904, 2019, doi: 10.1109/ACCESS.2019.2917886.
- [13] C. Beuter and M. Oleskovicz, "S-transform: from main concepts to some power quality applications," *IET Signal Processing*, vol. 14, no. 3, pp. 115–123, May 2020, doi: 10.1049/iet-spr.2019.0042.
- [14] N. E. Huang *et al.*, "The empirical mode decomposition and the Hubert spectrum for nonlinear and non-stationary time series analysis," in *Proceedings of the Royal Society A: Mathematical, Physical and Engineering Sciences*, Mar. 1998, vol. 454, pp. 903–995, doi: 10.1098/rspa.1998.0193.
- [15] S. Meignen and V. Perrier, "A new formulation for empirical mode decomposition based on constrained optimization," *IEEE Signal Processing Letters*, vol. 14, no. 12, pp. 932–935, Dec. 2007, doi: 10.1109/LSP.2007.904706.
- [16] N. Pustelnik, P. Borgnat, and P. Flandrin, "A multicomponent proximal algorithm for empirical mode decomposition," *European Signal Processing Conference*, pp. 1880–1884, 2012.
- [17] B. N. Harish and U. Surendra, "Power quality disturbance mitigation in grid connected photovoltaic distributed generation with plug-in hybrid electric vehicle," *International Journal of Electrical and Computer Engineering (IJECE)*, vol. 13, no. 6, pp. 6025–6036, Dec. 2023, doi: 10.11591/ijece.v13i6.pp6025-6036.
- [18] C. Aneesh, S. Kumar, P. M. Hisham, and K. P. Soman, "Performance comparison of variational mode decomposition over empirical wavelet transform for the classification of power quality disturbances using support vector machine," *Procedia Computer Science*, vol. 46, pp. 372–380, 2015, doi: 10.1016/j.procs.2015.02.033.
- [19] S. Boyd, *Distributed optimization and statistical learning via the alternating direction method of multipliers*. now Publishers Inc, 2010.
- [20] A. A. Abdoos, P. Khorshidian Mianaei, and M. Rayatpanah Ghadikolaei, "Combined VMD-SVM based feature selection method for classification of power quality events," *Applied Soft Computing Journal*, vol. 38, pp. 637–646, Jan. 2016, doi: 10.1016/j.asoc.2015.10.038.
- [21] L. Fu, T. Zhu, G. Pan, S. Chen, Q. Zhong, and Y. Wei, "Power quality disturbance recognition using VMD-based feature extraction and heuristic feature selection," *Applied Sciences*, vol. 9, no. 22, Nov. 2019, doi: 10.3390/app9224901.
- [22] K. Simonyan and A. Zisserman, "Very deep convolutional networks for large-scale image recognition," in *3rd International Conference on Learning Representations, ICLR 2015 - Conference Track Proceedings*, Sep. 2014, pp. 1–14.
- [23] H. Erişti, Ö. Yildirim, B. Erişti, and Y. Demir, "Automatic recognition system of underlying causes of power quality disturbances based on S-Transform and Extreme Learning Machine," *International Journal of Electrical Power and Energy Systems*, vol. 61, pp. 553–562, Oct. 2014, doi: 10.1016/j.ijepes.2014.04.010.
- [24] S. Wang and H. Chen, "A novel deep learning method for the classification of power quality disturbances using deep convolutional neural network," *Applied Energy*, vol. 235, pp. 1126–1140, Feb. 2019, doi: 10.1016/j.apenergy.2018.09.160.
- [25] O. Penangsang, M. D. Cahyonoputra, D. F. U. Putra, M. D. Faraby, S. Sofyan, and A. Muchtar, "Determination of location and capacity of distributed generations with reconfiguration in distribution systems for power quality improvement," *International Journal of Electrical and Computer Engineering (IJECE)*, vol. 13, no. 1, pp. 28–38, Feb. 2023, doi: 10.11591/ijece.v13i1.pp28-38.
- [26] N. Mohan, K. P. Soman, and R. Vinayakumar, "Deep power: deep learning architectures for power quality disturbances classification," in *2017 International Conference on Technological Advancements in Power and Energy (TAP Energy)*, Dec. 2017, pp. 1–6, doi: 10.1109/TAPENERGY.2017.8397249.
- [27] M. Kaur and D. Singh, "Multi-modality medical image fusion technique using multi-objective differential evolution based deep neural networks," *Journal of Ambient Intelligence and Humanized Computing*, vol. 12, no. 2, pp. 2483–2493, Aug. 2021, doi: 10.1007/s12652-020-02386-0.
- [28] Y. Xu and T. T. Qiu, "Human activity recognition and embedded application based on convolutional neural network," *Journal of Artificial Intelligence and Technology*, vol. 1, no. 1, pp. 51–60, Dec. 2021, doi: 10.37965/jait.2020.0051.
- [29] Y. Qiu, Z. Shen, Z. Shao, J. Shi, L. Xie, and J. Wu, "Comprehensive evaluation of power quality based on improved TOPSIS-RSR method," in *2021 China International Conference on Electricity Distribution (CICED)*, Apr. 2021, pp. 70–75, doi: 10.1109/CICED50259.2021.9556735.
- [30] X. Xi, P. Sun, C. Xing, S. Li, and X. Tian, "A parameter optimized variational mode decomposition method for harmonic and inter-harmonic detection," in *2023 IEEE 12th Data Driven Control and Learning Systems Conference (DDCLS)*, May 2023, pp. 1877–1882, doi: 10.1109/DDCLS58216.2023.10166482.
- [31] H. I. Hussein, A. Alazawi, A. Rodríguez, and F. Muñoz, "Performance evaluation of ST-based methods for simulating and analyzing power quality disturbances," *International Journal on Smart Sensing and Intelligent Systems*, vol. 16, no. 1, Jan. 2023, doi: 10.2478/ijssis-2023-0011.
- [32] Y. Wang, F. Liu, Z. Jiang, S. He, and Q. Mo, "Complex variational mode decomposition for signal processing applications," *Mechanical Systems and Signal Processing*, vol. 86, pp. 75–85, Mar. 2017, doi: 10.1016/j.ymsp.2016.09.032.
- [33] R. Martinez *et al.*, "Techniques to locate the origin of power quality disturbances in a power system: a review," *Sustainability (Switzerland)*, vol. 14, no. 12, p. 7428, Jun. 2022, doi: 10.3390/su14127428.
- [34] R. G. Stockwell, "A basis for efficient representation of the S-transform," *Digital Signal Processing: A Review Journal*, vol. 17, no. 1, pp. 371–393, Jan. 2007, doi: 10.1016/j.dsp.2006.04.006.
- [35] H. I. Hussein, A. M. Ghadhban, A. R. Gomez, and F. J. M. Gutiérrez, "Synthetic power quality disturbances generated by a mathematical model," in *4th International Conference on Current Research in Engineering and Science Applications, ICCRESA 2022*, Dec. 2022, pp. 65–70, doi: 10.1109/ICCRESA57091.2022.10352475.




**BIOGRAPHIES OF AUTHORS**

**Husham Idan Hussein**    was born in Baghdad, Iraq, in 1978, received his B.Sc. from the University Technology/Iraq in 2002, and M.Sc. from the University Technology of Malaysia (UTM) in 2012. He is currently a doctoral student at the University of Malaga School of Industrial Engineering Spain (2021-2022). His research interests are the optimization of power systems, power quality, power system state estimation, and renewable energy. He has many published papers. He can be contacted at email: 0611056898@uma.es.






**Ahmed Majeed Ghadban**    received the B.S. and M.S. degrees in power system engineering from the University of Technology, Iraq 2002, and the University of Technology Malaysia (UTM), Malaysia 2012, respectively. He is a doctoral student at the University of Malaga School of Industrial Engineering Spain (2021-2022). His current research interests are power system modelling, power stability, power reliability, and renewable energy. He can be contacted at email: 0611056851@uma.es.



**Alejandro Rodríguez Gómez**    an electrical and industrial management engineer, holds a master's in software engineering and AI, along with a Ph.D. in production systems engineering. Starting as a research fellow, he is now a professor at the University of Malaga School of Industrial Engineering, Spain, contributing to diverse projects. His research focuses on power quality, electromagnetic fields, and the electricity market, reflected in numerous international journals and books. He can be contacted at email: arodriguezg@uma.es.



**Francisco Jesus Muñoz Gutierrez**    is an electrical engineer and engineer in automation and industrial electronics, has a master's in software engineering and artificial intelligence and is a doctor from the University of Malaga following the mechatronics engineering program. He is currently a University Professor, having held the academic positions of secretary of the Department of Electrical Engineering, deputy director of the Polytechnic University School, and director of the Higher Polytechnic School of the University of Malaga. His topics of research include transmission lines and artificial intelligence techniques applied to power systems, electromagnetic pollution applications of genetic algorithms, signal quality, transients and time-frequency transforms. He can be contacted at email: fjmng@uma.es.